Available online at www.sciencedirect.com

SCIENCE DIRECT®

Nuclear Instruments and Methods in Physics Research A 555 (2005) 72–79

NUCLEAR INSTRUMENTS & METHODS IN PHYSICS RESEARCH Section A

www.elsevier.com/locate/nima

The effect of temperature on the rate capability of glass timing RPCs

D. González-Díaz[a], D. Belver[a], A. Blanco[b], R. Ferreira Marques[b,c], P. Fonte[b,d,*], J.A. Garzón[a], L. Lopes[b], A. Mangiarotti[e], J. Marín[f]

[a]*LabCaf, Departamento de Física de Partículas, Universidade de Santiago de Compostela, 15782 Santiago de Compostela, Spain*

[b]*LIP-Laboratório de Instrumentação e Física Experimental de Partículas, Departamento de Fisica, Universidade de Coimbra, 3004-516 Coimbra, Portugal*

[c]*Departamento de Física, Universidade de Coimbra, 3004-516 Coimbra, Portugal*

[d]*Instituto Superior de Engenharia de Coimbra, Rua Pedro Nunes, 3030-199 Coimbra, Portugal*

[e]*Physikalisches Institut der Universität Heidelberg, Philosophenweg 12, D-69120 Heidelberg, Germany*

[f]*CIEMAT, Avda. Complutense, 22-28040 Madrid, Spain*

Received 7 August 2005; received in revised form 7 September 2005; accepted 8 September 2005

Abstract

In this study, we demonstrate a strong influence of the working temperature on the counting rate capability of large-area timing resistive plate chambers (RPCs) incorporating industrial flat glass electrodes. The effect relies on the sharp dependence of glass resistivity on temperature, approximately one order of magnitude for each 25 °C, allowing a considerable extension of the counting rate capability merely by a moderate warming of the detector.

The results confirm operation at 1.5 kHz/cm^2 for irradiation with gamma photons, and may be extrapolated to 6 kHz/cm^2 for the detection of minimum ionizing particles (MIPs) with a timing resolution below 100 ps σ.

PACS: 29.40. Cs

Keywords: Gaseous detectors; RPC; Time-of-flight; Rate capability

1. Introduction

Resistive Plate Chambers (RPCs) with timing resolutions below 100 ps σ for minimum ionizing particles (MIPs) have been recently developed [1,2]. This type of detector, operating at atmospheric pressure with non-flammable gases, seems well-suited for high-granularity time-of-flight (TOF) systems, providing performances comparable to the scintillator-based TOF technology but offering a significantly lower price per channel, compact mechanics and magnetic field compatibility.

In practice, the counting rate capability of RPCs is strongly dependent on the availability of suitable resistive electrode materials. For many applications, the extension of the rate capabilities achievable with industrial glass electrodes, around 2 kHz/cm^2 [3], to higher values is of fundamental importance. Although one may consider the use of materials with much lower resistivity [4], for large area applications this approach is of questionable feasibility.

To address this issue, in this study we present a practical way to lower the resistivity of large-area timing RPCs made with industrial flat glass electrodes by exploiting the strong temperature dependence of the resistivity of many common glasses, correspondingly increasing the RPC rate capability [5].

2. Resistivity of industrial flat glass

It is known (see for instance Ref. [6]) that the resistivity ρ of many non-metallic conductors depends on temperature

*Corresponding author at: LIP-Laboratório de Instrumentação e Física Experimental de Partículas, Departamento de Fisica, Universidade de Coimbra, 3004-516 Coimbra, Portugal. Tel.: +351 239833465; fax: +351 239822358.

E-mail address: fonte@lipc.fis.uc.pt (P. Fonte).

0168-9002/$ - see front matter © 2005 Elsevier B.V. All rights reserved.
doi:10.1016/j.nima.2005.09.005

following the Arrhenius law

$$\ln(\rho) = a + \frac{b}{T}$$

which, for narrow temperature intervals, may be conveniently represented as

$$\rho \simeq \rho_{T_0} 10^{(T_0 - T)/\Delta T} \quad (1.1)$$

where ΔT is the temperature increase required for a resistivity decrease by one order of magnitude and, ρ_{T_0}, the resistivity at the reference temperature T_0.

A resistivity measurement of several glass types from common brands is shown in Table 1, evidencing a steep decrease of the resistivity by about one order of magnitude per 25 °C of temperature increase. It is remarkable that all glass types studied (see also Ref. [5]) show a similar behaviour in this aspect, evidenced by very similar ΔT parameters.

Naturally, as it was already shown experimentally for 2 mm-gap glass RPCs [5], it is to be expected that the counting rate characteristics of RPCs made from such glasses will improve when the glass temperature is increased. Therefore, it is interesting to study the practical use of Warmed timing RPCs, easily extending the counting rate capability, while keeping the practical advantages of using industrial flat glass for its construction.

Table 1
Measured resistivity data for several types of industrial flat glass

Manufacturer-type	Thickness (mm)	ρ_{20} ($10^{12}\,\Omega$ cm)	ΔT (°C)
Guardian-clear	1.8	9.55	24.6
Glaverbel-clear	1.9	10.5	24.3
Glaverbel-clear	0.4	7.03	23.5
Saint Gobain-clear	3.9	6.69	24.9
SCHOTT-D263T	0.3	494	23.9

The parameters are defined in accordance with Eq. (1.1): ΔT is the temperature increase required for a resistivity decrease by one order of magnitude and ρ_{20} is the resistivity at 20 °C.

3. Experimental set-up

The tests were performed on one of the four-gap shielded timing RPCs of $2 \times 60\,\text{cm}^2$ area, described in Refs. [7,8]. The gas enclosure was equipped with several internal thermometers and inserted in an external heating sleeve controlled by a temperature stabilization system. An illustration of the set-up can be seen in Fig. 1.

The internal temperature differences, measured over the RPC aluminium shield, were generally smaller than 1 °C, assuring that, under static conditions, the temperature of the enclosed RPCs would remain within these limits.

Both time and charge data were taken from each of the RPC extremities using an updated design of the electronics

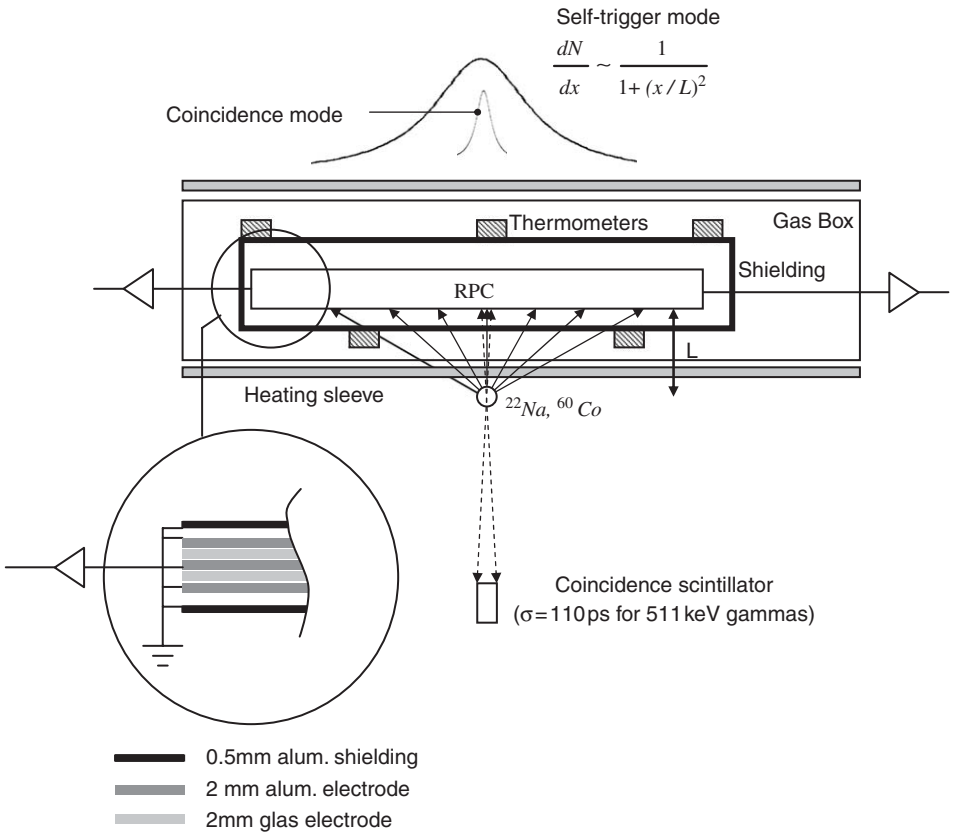

Fig. 1. Schematic representation of the test set-up. Irradiations were made with radioactive sources of ^{22}Na and ^{60}Co. The ^{22}Na positron annihilation source allows to perform timing measurements in coincidence with a scintillator.

described in Ref. [9]. The longitudinal position of the avalanche was calculated from the difference between the signal arrival times at both RPC extremities and a position-independent TOF information was calculated from the average of both arrival times, after correction for avalanche-size effects.

The avalanches were triggered by ^{22}Na or ^{60}Co gamma sources, considering two modes of operation.

In the self-trigger mode, data were taken upon detection of an avalanche anywhere in the RPC. From geometric considerations it can be seen that the intensity of the primary irradiation at each position follows, in this case, a Cauchy distribution

$$\phi_{\mathrm{p}}(x) = \frac{\phi_{\max}}{1 + (x/L)^2} \tag{1.2}$$

where x is the longitudinal position along the RPC (60 cm length) and, L, the RPC–source distance. In coincidence mode, a coincidence was required between the RPC and a narrow timing scintillator. Such events arise mainly from simultaneous anti-parallel 511 keV gamma photons emitted by the ^{22}Na positron annihilation source. The timing resolution of the scintillator was determined by a similar experiment where the coincidence was required between a pair of identical scintillators, yielding a value of 110 ps σ.

Table 2
Source combinations used in this work

Name	Description	Distance L (cm)	$\Phi_{\max}$ (kHz/cm^2)
A	0.5 mCi ^{22}Na + 0.6 mCi ^{60}Co	5	1.8
B	0.5 mCi ^{22}Na + 0.6 mCi ^{60}Co	7.5	0.8
C	0.5 mCi ^{22}Na	5	0.9
D	0.05 mCi ^{22}Na	5	0.08

All tests were performed using one of the source combinations listed in Table 2.

In all cases the measurements were performed as a function of the effective applied voltage

$$V_0^* = V_0 \frac{T}{T_{\mathrm{ref}}} \frac{P_{\mathrm{ref}}}{P} = V_0\, T^* \tag{1.3}$$

so as to keep constant the reduced applied field E/n (n being the gas density) when the pressure or temperature change.

4. Results

4.1. Avalanche charge distribution

While for the detection of MIPs, four-gap timing RPCs show a reasonably peaked charge distribution ([2], for instance), the situation is quite different when these detectors are irradiated with γ photons. The detection takes place rather indirectly, via the detection of a secondary electron that is ejected into the gas gap from the electrodes after a photoelectric, Compton or pair-producing interaction of the primary photon with the electrode material. Avalanches will be initiated along the path of the ejected electron, which features a broad energy spectrum and enters the gas gap at any angle, resulting in an essentially exponential avalanche charge distribution, as shown in Fig. 2.

The exponential shape of the charge distribution for γ irradiation indicates that, in this situation, the detection efficiency will be much more sensitive to small gain variations than in the case of MIPs. Therefore, one may conveniently use the visible count rate at a given position as a sensitive indicator of the rate-induced variations of the local gain.

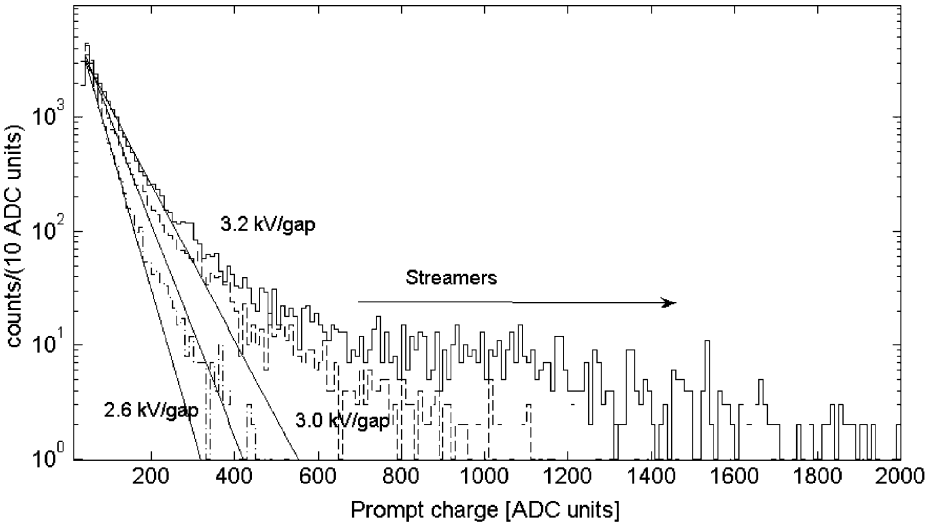

Fig. 2. When irradiated with gamma photons the timing RPC produces an essentially exponential charge distribution. The peak at small charges is caused by the electronics threshold, while the tail, at charges above ~500 units, is caused by "streamer" discharges. In this situation, the detection efficiency is much more sensitive to gain variations than for the detection of MIPs, where a shallow peak can be observed even in single-gap counters [10].

It is useful to note that for an exponential charge distribution the observable average charge $\bar{q}_{\rm obs}$ above a detection threshold $q_{\rm th}$ is given by

$$\bar{q}_{\rm obs} = \bar{q} + q_{\rm th}. \tag{1.4}$$

4.2. Timing accuracy

Timing measurements were performed by the method described in Section 3 as a function of the source intensity, effective applied voltage and working temperature, being the results shown in Fig. 3. Remarkably, none of these variables exerts any discernible effect on the timing accuracy, and a constant resolution around 90 ps σ is observed, in general agreement with previous measurements using γ photons [4].

4.3. Efficiency

As stated before, the efficiency of timing RPCs irradiated with γ photons should be particularly sensitive to variations of the operating parameters. Therefore, this quantity

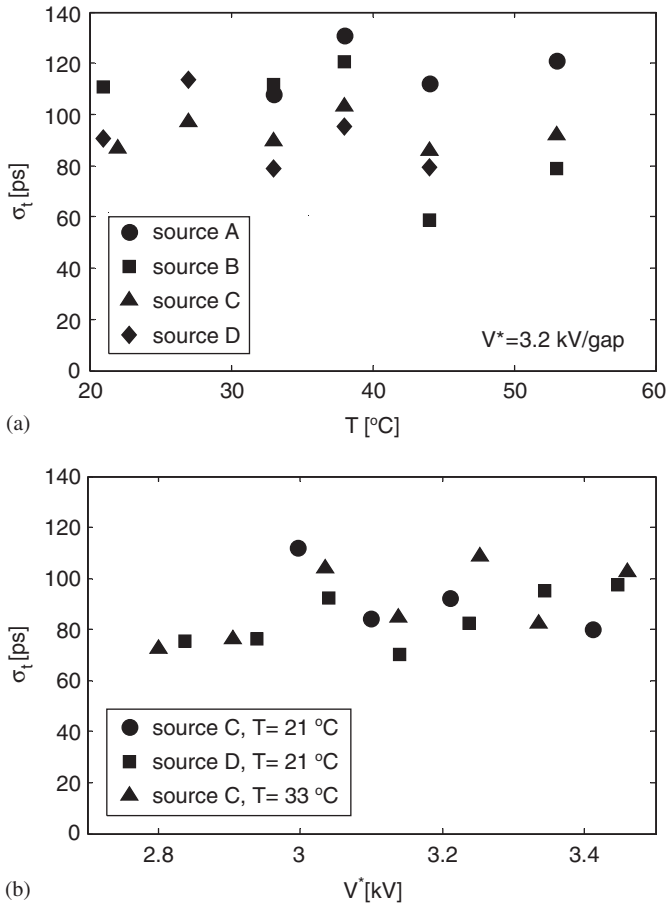

Fig. 3. Timing accuracy (ps σ) for 511 keV gamma photons as a function of the source intensity (see Table 2), effective applied voltage V^* (1.3) and working temperature T. Remarkably, none of these factors exerts any perceptible effect on the timing accuracy for gamma photons, in general agreement with previous observations [4].

may be more suitable than the timing resolution for an assessment of the effects of temperature on the counter. However, extraction of the relevant physical parameters from the data requires the development of a minimally realistic model of the detector efficiency. We adopted a simple model, related to the one described in Ref. [11], that captures the essential features of the RPC behaviour, without attempting to reach an exact description. The model is based on the following principles.

The primary intensity $\phi_{\rm p}(x)$ follows a Cauchy distribution as stated in Eq. (1.2).

The current per unit area at any position in the detector is proportional to the local average charge $\bar{q}$ (considering Eq. (1.4)) and to the local primary intensity

$$i(x) = b\,\phi_{\rm p}\,\bar{q}, \tag{1.5}$$

where b is a proportionality factor.

Close to the operating point, the local average charge depends linearly on the local difference between the effective gap voltage (compare with Eq. (1.3)) and a threshold-like voltage $V_{\rm th}$:

$$\bar{q} = a((V_0 - Ri)T^* - V_{\rm th}) = \bar{q}_0 - a\,Ri\,T^* \tag{1.6}$$

where $R = R(T)$ is the temperature-dependent glass resistance crossed by the counting current i (therefore, Ri represents the voltage drop across the glass), a is a proportionality factor and $\bar{q}_0$ is the average charge in the zero voltage drop limit. This approximate linear behaviour has been well established for RPCs at large gains, arising from the space charge saturated avalanche regime (see Ref. [11] for instance) and was also observed in the present case between 2.6 and 3.2 kV/gap.

The solution of the system of Eqs. (1.5) and (1.6) yields

$$\bar{q} = \frac{\bar{q}_0}{1 + k\phi_{\rm p}} \tag{1.7}$$

where all the temperature dependence is contained in

$$k(T) = a\,b\,T^*\,R(T). \tag{1.8}$$

For an exponential charge distribution (see Fig. 2) the detection efficiency for a detection threshold $q_{\rm th}$ is given by

$$\varepsilon = \mathrm{e}^{-q_{\rm th}/\bar{q}} \tag{1.9}$$

which, using Eq. (1.7), translates into

$$\varepsilon = \mathrm{e}^{-q_{\rm th}/\bar{q}_0}\,\mathrm{e}^{-(q_{\rm th}/\bar{q}_0)k\phi_{\rm p}}. \tag{1.10}$$

The observable counting rate at any position will be given as a function of the primary rate (1.2) by

$$\phi_{\rm obs} = \phi_{\rm p}\,\varepsilon = \phi_0\,\mathrm{e}^{-(q_{\rm th}/\bar{q}_0)k\phi_{\rm p}} \tag{1.11}$$

where we defined the quantity $\phi_0(x)$ as the local counting rate that would be observable in the zero glass resistance limit (absence of rate effects). Therefore, the model contains four temperature-independent parameters $\phi_{\max}$, L, $q_{\rm th}$ and $\bar{q}_0$, plus one parameter k_T for each temperature, totalling ten parameters in the present study.

The ϕ_{max} and L parameters are obtained from a fit to the observed counting rate distribution of the source D (weakest), while the remaining eight parameters are robustly determined by a global least-squares fit to the collected data, as shown in Figs. 4 and 5. In total, 84 individual curves were adjusted simultaneously.

Fig. 4(a) shows data on the observed local counting rate, while Fig. 4(b) shows avalanche prompt (electron component) charge data, both collected as a function of the avalanche position for different operating temperatures and radiation sources. The effective applied voltage was $V_0^* = 3.2\,\mathrm{kV}$ per gap. It seems clear that for the strongest sources there is a sharp increase of the observed counting rate with increasing temperature.

Fig. 5 presents similar data for different values of the effective operating voltage and a more restricted choice of radiation sources and temperatures.

Overall, it is apparent that the model describes reasonably, but not exactly, the observed RPC behaviour, as it should be expected from such a simple approach.

4.4. Rate capability

The exponential term in Eq. (1.11) represents the efficiency drop caused by rate. This term can be easily extracted from the data points shown in Fig. 4 by normalization and it is represented in Fig. 6.

The detector rate capability may be defined in a natural way as the primary rate Φ_p that corresponds to a certain rate-induced efficiency drop ε_Φ, yielding from (1.10)

$$\Phi_p(T) = c\frac{\ln(\varepsilon_\Phi)}{k} = \frac{d}{T^* R(T)} \tag{1.12}$$

where the constants c and d may be easily deduced from the definitions. This corresponds to the intersection of the model lines shown in the Fig. 6(a) with an horizontal line at height ε_Φ.

Furthermore, using Eq. (1.1), the rate capability would be expected to follow

$$\Phi_p(T) = c\frac{\ln(\varepsilon_\Phi)}{k} = \frac{d}{R_{T_0}}\frac{10^{(T-T_0)/\Delta T}}{T^*} \tag{1.13}$$

allowing a comparison between the values of k_T obtained from the fit with the direct measurements of the glass resistivity. It should be noted that relative variations of the rate capability (taking T_1 as a reference temperature)

$$\frac{\Phi_p(T)}{\Phi_p(T_1)} = \frac{k_{T_1}}{k_T} = \frac{T_1^*}{T^*}10^{(T-T_1)/\Delta T} \tag{1.14}$$

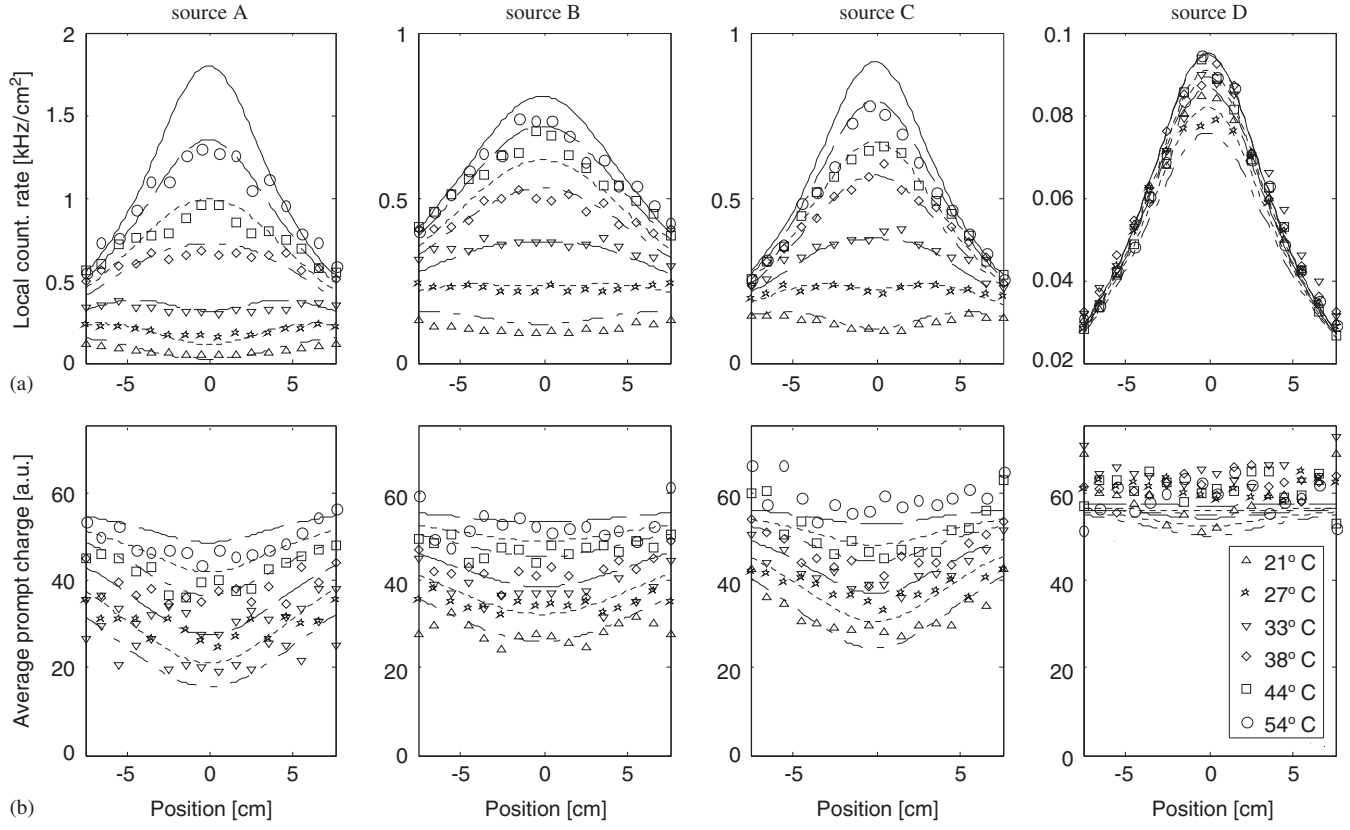

Fig. 4. Least-squares fit of the model described in the text (lines) to the observed local counting rates (a) and average prompt charge (b) as a function of the avalanche position in the central 14 cm of the RPC. Each column corresponds to one of the radioactive sources described in Table 2 and to different working temperatures. A sharp increase on the visible counting rate with increasing temperature is evident for the strongest sources (about 15-fold for source A). The upper line in (a) corresponds to the quantity ϕ_0 defined in Eq. (1.11). The effective applied voltage was in all cases $V_0^* = 3.2\,\mathrm{kV}$ per gap.

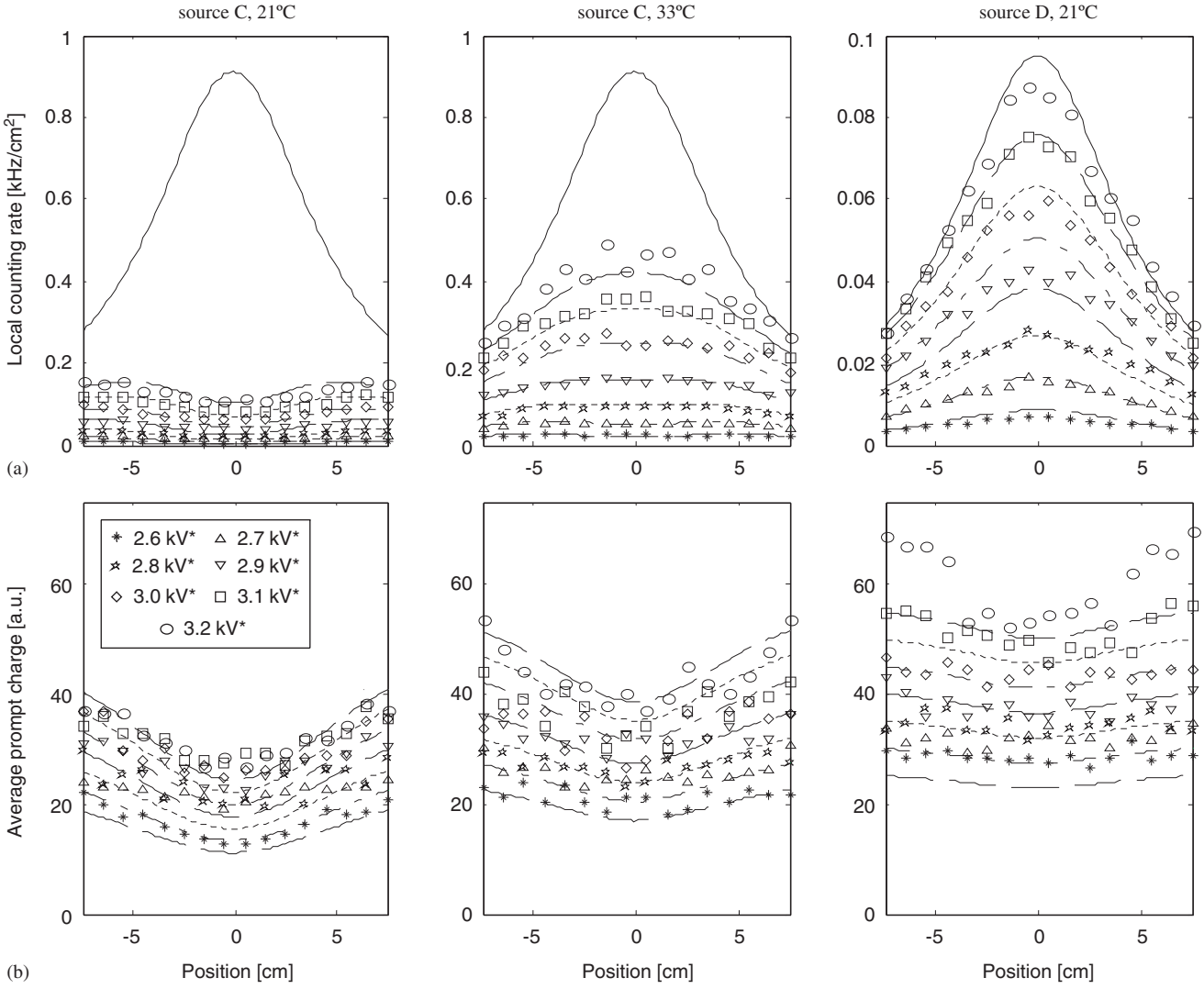

Fig. 5. Similar to Fig. 4, but for different values of the effective operating voltage and a more restricted choice of radiation sources and working temperatures.

depend only on T, T^*, k_T and ΔT, allowing a very clean evaluation of the effect of temperature on the rate capability. The quantities defined on the middle and right-hand side terms of Eq. (1.14) are represented in Fig. 7, evidencing a quite good mutual agreement and indicating a rate improvement by a factor 10 when the temperature is increased by 25.4 °C.

Based on these results, it is possible to extrapolate measurements made with the same counter on particle beams [8], suggesting that operation at resolutions below 100 ps σ and efficiencies of close to 90% may be feasible at 6 kHz/cm^2 (ten-fold increase) when the detector is operated close to 50 °C. A representation of this extrapolation is shown in Fig. 8 (straight line).

5. Background counting rate

A sharp increase of the background (dark) counting rate has been observed when the temperature is increased above 54 °C, as shown in Fig. 8 (see also Ref. [12]). However, it is a common observation that when voltage is applied on a new counter, or the operating conditions drastically changed, frequently there is a temporary increase of the dark current that subsides afterwards (a process commonly known as "conditioning") as is documented, for instance, in [13]. Therefore, the effect just described may be considered as a worst-case scenario.

Anyhow, at all temperatures considered, the dark count rate is negligible when compared to the expected maximum count rate, also shown in Fig. 8.

6. Conclusion

It was demonstrated in a large size timing RPC that a 25 °C temperature increase improves the count rate capability by one order of magnitude, extending the applicability of timing RPCs made with industrial flat glass to much larger counting rates merely by a moderate warming of the detector.

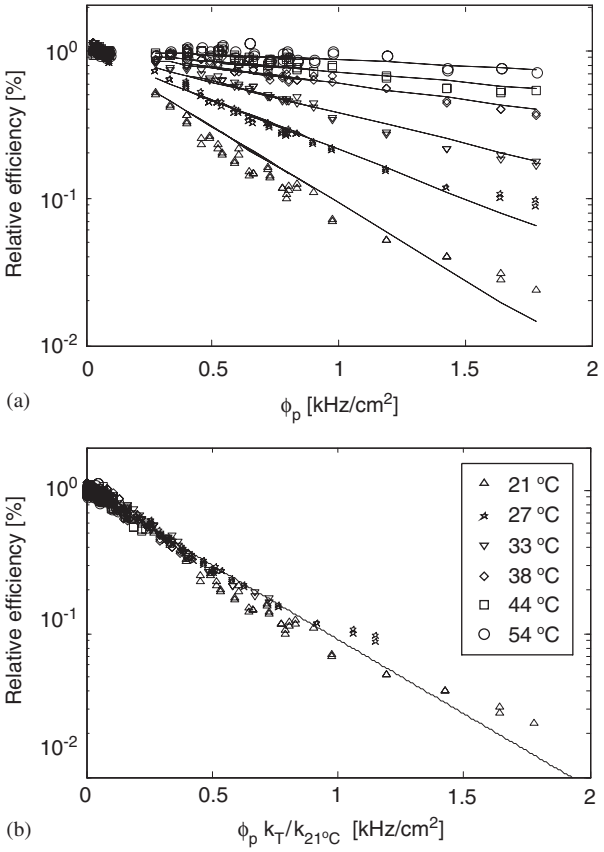

Fig. 6. (a) Relative efficiency drop as a function of the primary counting rate ϕ_p, derived from the data shown in Fig. 4, superimposed with the model curves derived from the fits shown in Figs. 4 and 5. (b) The same data is represented with the primary rate rescaled in accordance with the model (1.11), showing that all curves follow essentially the same exponential law.

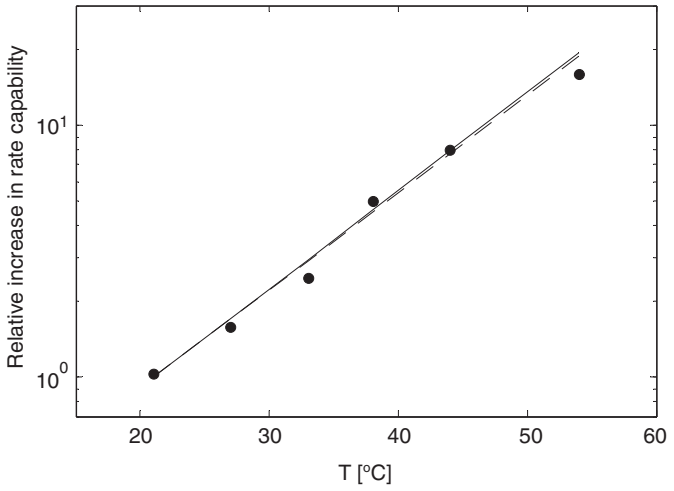

Fig. 7. Relative increase of rate capability with detector temperature, estimated by measurements of detector behaviour (dots: k_{T_1}/k_T following (1.14); solid line: exponential fit to these points) and by direct measurements of the glass conductivity (dashed line: rightmost term in (1.14)). A very good agreement between both measurements is evident, indicating a rate improvement by a factor 10 when the temperature is increased by 25.4 °C.

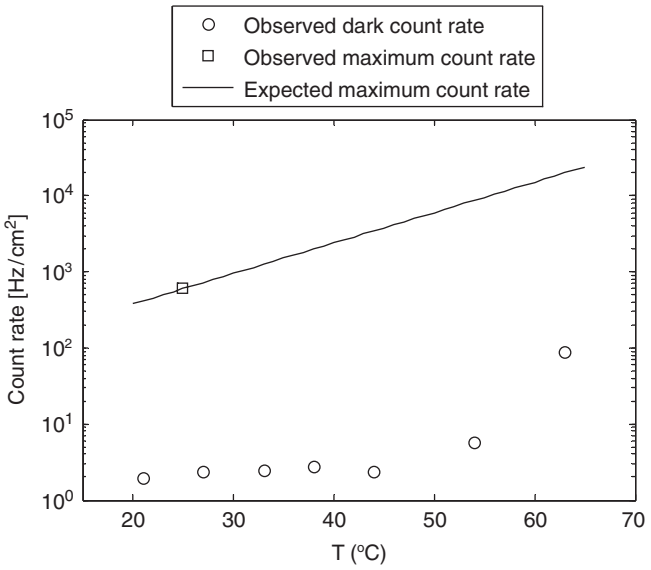

Fig. 8. Observed dark count rate and expected rate capability in particle beams (from [8], scaled to higher temperatures in accordance with Fig. 7). A sharp increase of the dark count rate is visible above 54 °C, remaining, however, much smaller than the expected maximum counting rate.

Reasonable extrapolation of results obtained in particle beams with the same counter at ambient temperature indicates that operation at 6 kHz/cm^2 may be feasible around 50 °C.

Naturally, further research is required on issues like temperature control of large RPC systems, dark count rate, detector aging and materials compatibility.

Acknowledgements

This work was co-financed by the Fundação para a Ciência e Tecnologia projects CERN/FNU/43723/2001, POCTI/FP/FNU/50171/2003, FEDER, MCYT FPA2000-2041-C02-02, FPA2003-7581-C02-02, XUGA PGIDT-02-PXIC-20605-PN, the EU 6th Framework Program via contract RII3-CT-2003-506078 and the program INTAS 03-54-3891.

We benefited from the competent technical work of N. Carolino, N. Montes, A. Pereira and M. Zapata.

D. González-Díaz gratefully acknowledges the hospitality received at the University of Heidelberg, Germany.

References

[1] P. Fonte, A. Smirnitski, M.C.S. Williams, Nucl. Instr. and Meth. A 443 (2000) 201.
[2] P. Fonte, et al., Nucl. Instr. and Meth. A 449 (2000) 295.
[3] A. Akindinov, et al., Nucl. Instr. and Meth. A 490 (2002) 58.
[4] L. Lopes, R. Ferreira Marques, P. Fonte, A. Pereira, V. Peskov, A. Policarpo, Nucl. Instr. and Meth. A 533 (2004) 69.
[5] C. Gustavino, A. Candela, M. De Deo, M. D'Incecco, N. Redaelli, A. Tonazzo, G.C. Trinchero, Nucl. Instr. and Meth. A 527 (2004) 471.
[6] J. Zarzycki, Glasses and the Vitreous State, Cambridge University Press, Cambridge, 1991.
[7] H. Alvarez-Pol, R. Alves, A. Blanco, N. Carolino, J. Eschke, R. Ferreira Marques, P. Fonte, A. Pereira, J. Pietraszko, J. Pinhão, A. Policarpo, J. Garzon, D. González-Díaz, J. Stroth, Nucl. Instr. and Meth. A 533 (2004) 79.
[8] H. Alvarez-Pol, R. Alves, A. Blanco, N. Carolino, J. Eschke, R. Ferreira Marques, P. Fonte, A. Pereira, J. Pietraszko, J. Pinhão, A. Policarpo, J. Garzon, D. González-Díaz, J. Stroth, Nucl. Instr. and Meth. A 535 (2004) 277.
[9] A. Blanco, N. Carolino, P. Fonte, A. Gobbi, IEEE Trans. Nucl. Sci. NS-48 (2001) 1249.
[10] P. Fonte, V. Peskov, Nucl. Instr. and Meth. A 477 (2002) 17.
[11] G. Carboni, G. Collazuol, S. De Capua, D. Domenici, G. Ganis, R. Messi, G. Passaleva, E. Santovetti, M. Veltri, Nucl. Instr. and Meth. A 498 (2003) 135.
[12] G. Aielli, et al., Nucl. Instr. and Meth. A 508 (2003) 44.
[13] L. Lopes, R. Ferreira-Marques, P. Fonte, A.P. Piedade, A. Policarpo, Nucl. Instr. and Meth. A 533 (2004) 121.